JAREE (2026), Vol. 10, No. 1
doi: 10.12962/jaree.xyzxyz

Journal on Advanced Research in Electrical Engineering
ISSN: 2579-6216

RESEARCH ARTICLE

Improved Surge Speed Adaptive Line-of-Sight Guidance Law in Current Disturbance Environment for Unmanned Surface Vehicle

Muhammad Alifuddin Akbar [1] , Mochammad Sahal*, Abdullah Alkaff

[1] Department of Electrical Engineering, Institut Teknologi Sepuluh Nopember, Surabaya, Indonesia

*Corresponding author (sahal@its.ac.id).

Received: 31 May 2025; **Revised:** 29 July 2025 **Accepted:** 31 July 2025

Abstract

This work proposes a method for calculate the surge speed reference integrated with an Adaptive Line-of-Sight (ALOS), called Improved Surge Speed Adaptive Line-of-Sight (ISS-ALOS), to enhance the path following performance of Unmanned Surface Vehicle (USV). This method utilizes ALOS guiding law to enable the USV to maintain the desired path regardless of disturbances. The proposed ISS-ALOS uses the path's curvature, cross-track error (XTE), and XTE rate to calculate the surge speed reference. The method is applied to USV following a curved path with several bends and a square path with sharp turns, to demonstrate with high reliability that the proposed method can direct the USV along the specified path with minimum XTE. Compared to the existing approaches, the ISS-ALOS achieves lower XTE root mean square error (RMSE), with a 3.68% improvement on the curved path and 2.89% improvement on the square path, confirming its superior path following accuracy.

Keywords: cross-track error, guidance law, path following, surge speed, unmanned surface vehicle.

I. Introduction

Unmanned Surface Vehicle (USV) is a water vessel that can operate autonomously or remotely on the water's surface without a human crew. A guidance system is necessary for the USV to operate independently. The guidance system is helpful when the USV motion control task requires the USV to follow a predefined path.

Path following is one of the common scenarios discussed in USV motion control. The fact that USVs are typically underactuated systems, meaning there are fewer actuators than degrees of freedom (DOF), is what frequently causes issues in path following. Surge and yaw are the only two that have control inputs that generate motion in the USV's three degrees of freedom (surge, sway, and yaw), which results in coupled and nonlinear states [1].

The line-of-sight (LOS) method imitates the directional command of an experienced sailor to ensure convergence to the intended course. The conventional approach that became the basis for the development of LOS is proportional LOS (PLOS). The PLOS method has the disadvantage that if the vessel is exposed to unknown external disturbances, such as currents, wind, and waves, it can cause the USV to deviate from the correct path. A difference between the ship's heading and speed direction, known as the sideslip angle, can result from drift forces caused by these external disturbances [2].

Various approaches have been developed to overcome the drift force caused by external disturbances. The integral term was introduced in [3] to compensate for the unknown ocean current to create Integral LOS (ILOS). Reference [4] improved the method further to create Adaptive Integral LOS (ALOS) which takes the sideslip angle as the constant parameter to be estimated. Then, ALOS was improved in [5] to avoid using an arctangent function during the computation of sideslip angle compensation, which could lead to saturation of the compensation.

ILOS and ALOS have several limitations, such as only working effectively to compensate for a constant sideslip angle. To address this issue, an LOS based on the Extended State Observer (ESO) was developed. Reference [6] employs a reduced-oder ESO to estimate the sideslip angle by utilizing an auxiliary state in the observer. The method is referred to as the Extended State Observer LOS (ELOS).

After that, the LOS approach described above encountered several of improvements. To address the situation of time-varying sideslip and time-varying ocean current using ALOS, for instance, an Improved Adaptive Integral LOS (IAILOS) was developed in [7]. In [8], an Improved ELOS based on ELOS was developed, which can eliminate the presumption that the sideslip angle is small. Reference [9] demonstrates the use of an Augmented Extended Kalman Filter (AEKF) to estimate tracking error and sideslip angle in conjunction with the LOS guidance law to to accomodate a small sideslip angle assumption.

Further improvement of guidance performance is adjusting the lookahead distance to a variable with adjustable values. The time-varying lookahead distance was first introduced in [10], where its value is determined by an exponential function based on the cross-track error (XTE). Reference [11] proposed fuzzy logic with inputs of XTE and the rate of XTE to compute the lookahead distance in combination with ILOS was demonstrated. The computation of time-varying lookahead distance based on XTE and course speed, combined with the Improved ILOS guidance law, was shown in [12]. Reference [13] calculated the lookahead distance using fuzzy logic with XTE and XTE rate as inputs,

How to cite: Akbar, M. A., Sahal, M., & Alkaff, A. (2026). Improved Surge Speed Adaptive Line-of-Sight Guidance Law in Current Disturbance Environment for Unmanned Surface Vehicle. JAREE (Journal on Advanced Research in Electrical Engineering), Volume 10 (No.1).

and utilized an ESO-based ILOS (EILOS) as the guidance law. ALOS was demonstrated in [14] as a guidance law with sideslip compensated using reduced-order ESO and the time-varying lookahead distance was computed based on course speed and XTE.

Another approach that can be used to improve guidance performance is to adjust the USV's surge speed reference. The Heading-Surge (HS) guidance scheme was used in [15] to calculate the surge speed reference based on XTE and lookahead distance with a guidance law using the LOS approach. Reference [16] presents a similar calculation to determine the surge speed reference, using Improved ELOS as the guidance law and the lookahead distance as a variable that varies based on the along-track error (ATE). The hyperbolic tangent function is used in [17] to calculate the surge speed reference based on the XTE value, along with Finite-Time LOS (FTLOS) acts as the guidance law. A continuous path has a curvature; hence, the surge speed reference can be calculated using the path's curvature along with the LOS guidance law and sideslip estimated using ESO as proposed in [18]. The calculation of surge speed reference based on XTE and ATE with the guidance law using fixed-time dual adaptive line-of-sight (FTDALOS) is proposed in [19].

This study proposes Improved Surge Speed Adaptive LOS (ISS-ALOS). In ISS-ALOS, the surge speed reference is based on the path curvature, XTE, and rate of XTE, each of which is calculated using a hyperbolic tangent function. The surge speed reference calculation is then combined with the ALOS guidance law, which aims to improve the guidance capability of the USV.

This paper is organized as follows: Section II contains the USV model and tracking error calculation. Section III describes ISS-ALOS. Section IV presents simulation results and comparison with surge speed reference calculation in [19] and Section V is the conclusion.

II. Problem Formulation

A. Underactuated USV's Model

The USV movement model can be constructed from dynamics and kinematics equations. The dynamics equation is related to the forces that affect the movement of the USV in the body frame and the kinematics equation is related to the velocity transformation between the body frame to the North-East frame [20]. A three DOF USV's kinematics is given as

$$\begin{bmatrix}\dot{x}\\ \dot{y}\\ \dot{\psi}\end{bmatrix} = \begin{bmatrix}\cos(\psi) & -\sin(\psi) & 0\\ \sin(\psi) & \cos(\psi) & 0\\ 0 & 0 & 1\end{bmatrix}\begin{bmatrix}u\\ v\\ r\end{bmatrix}, \tag{1}$$

where x, y represent north-east position of USV and ψ is the heading angle from north axis. The linear velocities of surge and sway are denoted by u and v. The yaw angular velocity is denoted by r. The variables u, v and r are expressed in body frame.

Let the relative velocity vector in the body frame be represented by $\nu_r = [u_r \quad v_r \quad r_r]^T$. With $\nu_c = [u_c \quad v_c \quad 0]^T$ being the current velocity vector in the body frame, ν_r can be computed using the formula $\nu_r = \nu - \nu_c$. Therefore, the speed over ground can be computed using $\nu = \nu_r + \nu_c$. Using ν_r as defined, the general equation of USV dynamics is given by

$$M\dot{\nu}_r + C\nu_r + D = \tau \tag{2}$$

Inertia and coriolis-centrifugal matrices including rigid body and added mass are M and C given by (3) and (4).

Let m represent the mass of the rigid body, x_g denote the displacement from the origin to the center of gravity along the X-axis of the USV, and I_z denote the moment of inertia along the z-axis of the USV.

$X_{\dot{u}}, Y_{\dot{v}}, Y_{\dot{r}}, N_{\dot{v}}, N_{\dot{r}}$ represents the inertia added mass element. Added mass refers to the additional inertia received to a system due to its need of displacing certain amounts of fluid as the USV changes its velocity in the water.

$$M = \begin{bmatrix}m & 0 & 0\\ 0 & m & mx_g\\ 0 & mx_g & I_z\end{bmatrix} + \begin{bmatrix}X_{\dot{u}} & 0 & 0\\ 0 & Y_{\dot{v}} & Y_{\dot{r}}\\ 0 & N_{\dot{v}} & N_{\dot{r}}\end{bmatrix} \tag{3}$$

$$\begin{aligned} C &= \begin{bmatrix}0 & -mr & -mx_g r\\ mr & 0 & 0\\ mx_g r & 0 & 0\end{bmatrix} \\ &+ \begin{bmatrix}0 & 0 & Y_{\dot{v}}v_r + Y_{\dot{r}}r\\ 0 & 0 & -X_{\dot{u}}u_r\\ -Y_{\dot{v}}v_r - Y_{\dot{r}}r & X_{\dot{u}}u_r & 0\end{bmatrix} \end{aligned} \tag{4}$$

D is related to the linear and nonlinear damping forces. D can be written as

$$D = \begin{bmatrix}X_u u_r\\ Y_v v_r\\ N_r(1 + 10|r_r|r_r)\end{bmatrix} + \begin{bmatrix}0\\ Y_h\\ N_h\end{bmatrix} \tag{5}$$

where X_u, Y_v, and N_r are hydrodynamic damping constant. Y_h and N_h are crossflow damping whose values depend on the USV's relative velocity. Crossflow damping is the damping force caused by the flow of water crossing the hull. The input control vector produced by the actuator is $\tau = [\tau_x \quad 0 \quad \tau_\psi]^T$. A zero-valued input control exists because the USV is an underactuated system.

B. Tracking Error Calculation

Tracking error calculation is based on the Serret-Frenet (SF) frame traveling along a path. Let θ be the path parameter and the path is defined by the point which is a function of θ. If $(x_d(\theta), y_d(\theta))$ is the position where the USV is required and the path tangential at that point can be calculated by $\alpha = \mathrm{atan2}(y'(\theta), x'(\theta))$, then the following (6) can be used to calculate the tracking error in the form of ATE and XTE.

$$\begin{bmatrix}x_e\\ y_e\end{bmatrix} = \begin{bmatrix}\cos(\alpha) & \sin(\alpha)\\ -\sin(\alpha) & \cos(\alpha)\end{bmatrix}\begin{bmatrix}x - x_d\\ y - y_d\end{bmatrix}, \tag{6}$$

where x_e denote ATE and y_e denote XTE. ATE and XTE are the parallel and perpendicular distances, respectively, between the USV and the required position. The illustration of XTE, ATE, and the overall geometrical principle of LOS guidance Law is shown in Fig. 1. In this figure, Δ is the lookahead distance and α is the tangential path.

III. Improved Surge Speed Adaptive LOS

This section establishes the heading reference computed by ALOS same shown in [5] and the surge speed reference determined by path curvature, XTE, and the rate of change of XTE.

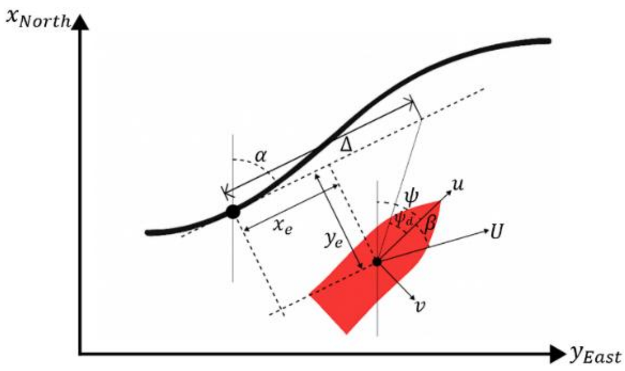

Fig. 1. Geometrical Principle of LOS Guidance

The sideslip angle in ALOS is regarded as a constant to be approximated by $\hat{\beta}$, with the estimated value acting for reducing the disturbances encountered by the USV. The computation of heading angle and $\hat{\beta}$, are given by the following equations:

$$\psi_d = \alpha - \tan^{-1}\left(\frac{y_e}{\Delta}\right) - \hat{\beta}_h, \quad \dot{\hat{\beta}}_h = \frac{k_{LOS}\,\Delta\; y_e}{\sqrt{(\Delta^2 + y_e^2)}}, \tag{7}$$

where k_{LOS} is an adaptation parameter that affects the aggressiveness of the ALOS value; an excessively large value could decrease the performance of the USV path following system, whereas an excessively small value may impair the system's ability to compensate for disturbances. Consequently, selecting the appropriate value for the adaptation parameter is crucial.

The surge speed reference is typically regarded as constant, or it is presumed that the force exerted along the surge axis maintains a set value. To enhance the performance of the path following USV, it is essential to adjust the surge speed reference according to specific situations. This study proposes that the surge speed reference varies according to path curvature, XTE, and the rate of change of XTE, as designated in the following equation

$$u_{ref} = u_{min} + \frac{\Delta_u}{2}(1 - \tanh(k_1\kappa)) + \frac{\Delta_u}{2}(\tanh(k_2 y_e^2)) - k_3 y_e \tanh(k_4 \dot{y}_e) \tag{8}$$

where u_{min} represents the minimum surge speed reference, while Δ_u denotes the expected deviation in the surge speed reference, y_e and $\dot{y}_e$ represent the XTE and its rate of change, respectively, whereas κ denotes the path curvature as determined by

$$\kappa = \frac{|x'(\theta)y''(\theta) - x''(\theta)y'(\theta)|}{[x'^2(\theta) + y'^2(\theta)]^{3/2}} \tag{9}$$

The user-defined positive gain constants k_1, k_2, and k_4 determine the sensitivity of changes in κ, y_e, and $\dot{y}_e$ to changes in the surge speed reference, respectively. Additionally, k_3 is a positive gain constant that determines the effect of the correlation between y_e and $\dot{y}_e$, as shown in the fourth term, on the change of the surge speed reference. The larger value of k_3, the greater the change in the surge speed reference that can be caused by the fourth term. The second term in (8) relies on the assumption that path curvature substantially affects the motion characteristics of the USV, especially its capacity to keep on the desired path properly. The greater the curvature value of a path, the more signified its bend at a certain point; conversely, as the curvature approaches zero, the path becomes increasingly straight at that point. When the curvature is zero the path is entirely straight at that point. On a linear path, the curvature remains zero at every point along the path.

The greater the curvature of the path, the lower the velocity necessary for the USV to ensure effective path following. If the USV travels too fast along a curved path, it have difficulty to maintain its course, thereby diminishing path following performance. This strategy mimics humans who generally decrease velocity when maneuvering a sharp curve.

According to the aforementioned assumption, the increase of the surge speed reference in the second term is maximized when travelling on a straight path, namely $\lim_{\kappa\to 0}\frac{\Delta_u}{2}(1 - \tanh(k_1\kappa)) \approx \frac{\Delta_u}{2}$. As the curve on the path narrows, the surge speed reference in the second term is minimized, namely $\lim_{\kappa\to\infty}(1 - \tanh(k_1\kappa)) \approx 0$.

The third term in (8) is predicated on the idea that when the USV is a distant away from the path, either to the left ($y_e < 0$) or to the right ($y_e > 0$), the XTE increases in value. To speed up the USV's return to the intended path, an increased surge speed reference is necessary when the XTE increases, namely $\lim_{y_e\to\infty}\frac{\Delta_u}{2}(\tanh(k_2 y_e^2)) \approx \lim_{y_e\to-\infty}\frac{\Delta_u}{2}(\tanh(k_2 y_e^2)) \approx \frac{\Delta_u}{2}$. As the USV gets closer the desired path, the surge speed reference is decreased in order to avoid overshoot of the XTE, namely $\lim_{y_e\to 0}\frac{\Delta_u}{2}(\tanh(k_2 y_e^2)) \approx 0$.

In the fourth term, when the USV is positioned to the right of the path ($y_e > 0$) and moving away from the desired path ($\dot{y}_e > 0$), this term acts to decrease the surge speed reference, $-k_3 y_e \tanh(k_4 \dot{y}_e)$. When the USV approaches the desired path ($\dot{y}_e < 0$), the fourth term acts to increase the surge speed reference, $k_3 y_e \tanh(k_4 \dot{y}_e)$. If the USV lies on the left side of the path ($y_e < 0$), the fourth term functions analogously. The fourth term decreases the surge speed reference when the USV moves away from the desired path ($\dot{y} < 0$) and increases it when the USV closer to the desired path($\dot{y} > 0$). When the

USV is precisely on the desired path, the third and fourth terms become zero, thus have no impact on the surge speed reference.

IV. SIMULATION RESULT

A simulation was conducted to illustrate the performance and effectiveness of the ISS-ALOS, and to compare its performance to calculation based on [19]. The simulation utilizes the USV Otter parameter model from the MATLAB Marine System Simulator (MSS) Toolbox [20], with parameters detailed in Table I. These variables correspond to the physical and hydrodynamic parameters explained in Section II.A, particularly those used in the inertia and coriolis matrices defined in (3) and (4). The USV Otter is a catamaran-type USV, characterized by its two hulls positioned on either side of its central structure.

TABLE I. USV OTTER MODEL PARAMETER VALUES

Parameter (units)	Value
m (kg)	55
x_g(m)	0.2
I_z(kg m^2)	18.15
$X_{\dot{u}}$ (kg)	5.28
$Y_{\dot{v}}$ (kg)	1
$Y_{\dot{r}}$ (kg)	0
$N_{\dot{v}}$ (kg)	0
$N_{\dot{r}}$ (kg)	27.12

The USV Otter is equipped with two propellers located in the rear of each hull. To perform a turn, the USV adjusts the speed of one propeller to go faster than the rate of the other, while to maintain a straight direction, both propellers have been adjusted to operate at same rates.

The USV system in this simulation comprises numerous parts. The guidance system, including the ALOS guidance law computations and Improved Surge Speed (ISS), yielded the heading angle and surge speed reference. The outcomes of the guidance system calculations are subsequently compared with the actual states in the heading controller and speed controller. The surge speed reference compared with the actual surge speed, and the heading angle reference compared with the actual heading angle, resulting in surge error and heading error, respectively.

The surge error value, denotes with e_u, utilized by the PID controller within the speed controller to generate the appropriate τ_u value with K_p = 250, K_i = 25, and K_d = 0.1. The PID gains for the speed controller were tuned manually using a trial-and-error approach, where a step input was applied to the surge speed reference and the system's response was observed. The selected values ensure minimal or no steady-state error and limited overshoot, providing reliable surge speed tracking. The PID controller is

$$\tau_x = K_p e_u + K_i \int e_u dt + K_d \frac{de_u}{dt} \tag{10}$$

Meanwhile, the heading error, expressed as e_ψ, used in the heading controller, which is a PID controller similar to the speed controller but with different inputs and gain parameters. In the heading controller, K_p = 93.2, K_i = 13.97, and K_d = 82.95 are utilized to produce an appropriate τ_ψ.

The output of both controllers, must be processed for allocation to each propeller to achieve the necessary values for each rotation rate. The expected propeller rates computation is

$$n_d = \text{sign}(A\tau)\sqrt{A\tau} \tag{11}$$

Let $n_d \in \mathbb{R}^{2\times1}$ represent the expected propeller rates, comprises n_{d1}, which denotes the expected rates for the left propeller, and n_{d2}, which denotes the expected rates for the right propeller, $A \in \mathbb{R}^{2\times2}$ denotes the thrust configuration matrix, and $\tau \in \mathbb{R}^{2\times1}$ represent the output of the speed and heading controller calculations. The target value n_d used as a reference for actuator dynamics, and the actual propeller rates are denoted as n, with n_1 representing the actual speed of the left propeller and n_2 representing the actual speed of the right propeller. These actual propeller values are then used in dynamic and kinematic calculations to determine the USV states. The aforementioned scheme is illustrated in Fig. 2.

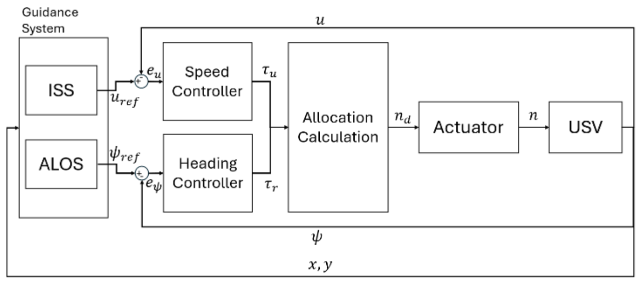

Fig. 2. USV Otter Simulation Scheme

The simulation involved testing throughout a continuous curved path defined by the functions $x(\theta)$ and $y(\theta)$, as well as along a square path created by linking waypoints with straight lines. The ISS-ALOS results compared with constant surge speed reference u = 1.5 m/s and the surge speed reference computations from [19], which was subsequently known as He Bu, utilizing the identical heading angle reference computation approach through the ψ_d calculation as described in (7). The ALOS parameter used in this test are k_{LOS} = 0.005 and Δ = 10 m. The computation of the surge speed reference presented in He Bu is illustrated as

$$u_d = k_u \sqrt{u_{d_{min}}^2 + k_{d1} x_e^2 + k_{d2} y_e^2} \tag{12}$$

A. Curved Path Trajectory

The curve path trajectory in this test was generated using the functions $x(\theta)$ and $y(\theta)$ as defined as

$$\begin{aligned} x(\theta) &= 10\theta \\ y(\theta) &= \theta + 200\sin^2(0.1\theta) + 150\sin(0.3\theta) \\ &\quad + 100\sin(0.05\theta) \end{aligned} \tag{13}$$

where θ represents the path parameter. This path shape was chosen due to its ability to provide a wavy path with various curvature degrees.

This test used a disturbance that consists of a water current traveling at a constant speed of $0.5\ \mathrm{m/s}$ at an angle of $\pi/6$ radians relative to the north axis. The initial body speed of the USV in this test is $\nu(0) = [0.1 \quad 0 \quad 0]^T$ while the initial location and orientation are $\eta(0) = [0 \quad 0 \quad 0]^T$. The ISS-ALOS parameters utilized in this test are presented in Table II, whereas the parameters utilized in He Bu are displayed in Table III.

The results of the trajectory formed from each calculation method are shown in Fig. 3. The tests demonstrate that the ISS-ALOS calculation can assists the USV to navigate the desired path, with several moments indicating that ISS-ALOS brings the USV nearer to the targeted path than using other surge speed reference calculation. This can be better noticed by observing the XTE plot shown in Fig. 4.

TABLE II. ISS-ALOS SURGE SPEED REFERENCE PARAMETER

Parameter	Value
u_{min}	0.75
Δ_u	1.5
k_1	4
k_2	0.01
k_3	0.75
k_4	0.5

TABLE III. HE BU [19] SURGE SPEED REFERENCE PARAMETER

Parameter	Value
k_u	1
$u_{d_{min}}$	0.75
k_{d1}	0.2
k_{d2}	0.01

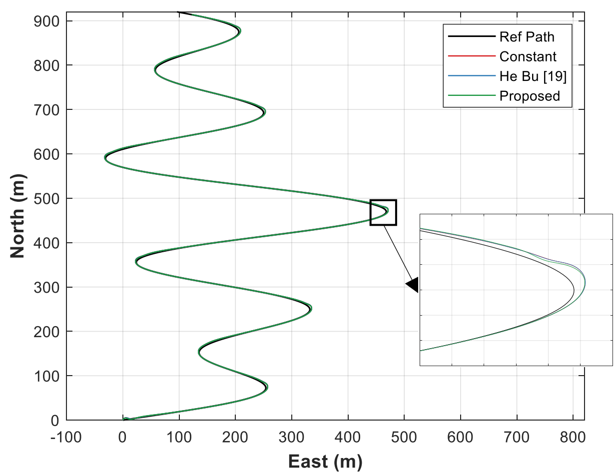

Fig. 3. Curved Path Trajectory Result

As can be observed, using ISS-ALOS can yield a reduced XTE than using other methods in the first 10 seconds when the USV begins to follow the path. The proposed equation demonstrates a clear advantage when the path changes direction, potentially resulting in significant XTE. The implementation of the ISS-ALOS can reduce the magnitude of the XTE as seen in the intervals 400-450 s, 600-700 s, and 900-1000 s. Table IV presents the RMSE, MAE, standard deviation, and maximum value of XTE on curved path trajectory.

Fig. 5 illustrates the comparison between the reference surge speed and the actual surge speed for each method. The reference values correspond to the outputs of the ISS-ALOS block as shown in Fig. 2. In certain sections, ISS-ALOS yields a significant surge speed value. This behavior due to the significant and rapid alteration of XTE.

The curvature of the path significantly influences the surge speed reference in ISS-ALOS. Specifically, when the path bends, the speed is reduced. At the proposed reference value for the surge speed reference, there is a nine times decrease in speed related to the turn in the path.

With the plot displayed in Fig. 6, the surge speed error can be computed from the comparison of the reference and actual surge velocities. The error of ISS-ALOS is notably large in certain areas, related to its increased surge speed reference when returning to the path. The surge speed reference value obtained from ISS-ALOS is highly variable, as it is influenced by the diverse conditions encountered by the USV. Consequently, its dynamics cannot directly follow to the specified reference, resulting in an increased error margin.

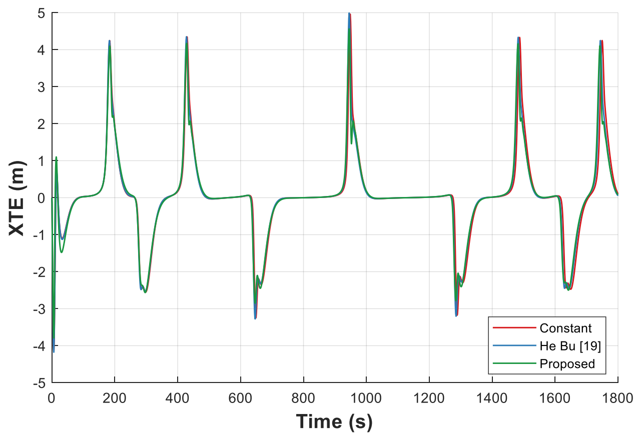

Fig. 4. XTE Plot of Curved Path Trajectory

TABLE IV. XTE NUMERIC VALUE

Method	RMSE (m)	MAE (m)	STD (m)	MAX (m)
Constant	1.176	0.629	1.175	4.961
He Bu [19]	1.168	0.628	1.167	4.991
Proposed	1.125	0.626	1.125	4.562

The relatively larger surge speed error in ISS-ALOS results from its adaptive surge speed referece strategy, which prioritizes minimizing XTE. This approach deliberately accepts larger speed error as a trade-off, as surge speed error is not the main performance measure in the guidance objective.

Table V presents the RMSE, MAE, standard deviation, and maximum value of the surge speed error. The maximum value for error surge speed data is observed between 100 s and its end. This is due to the fact that while the vehicle is just getting started, the surge speed error value so high that it is unable to accurately reflect the highest value of the test's actual surge speed error.

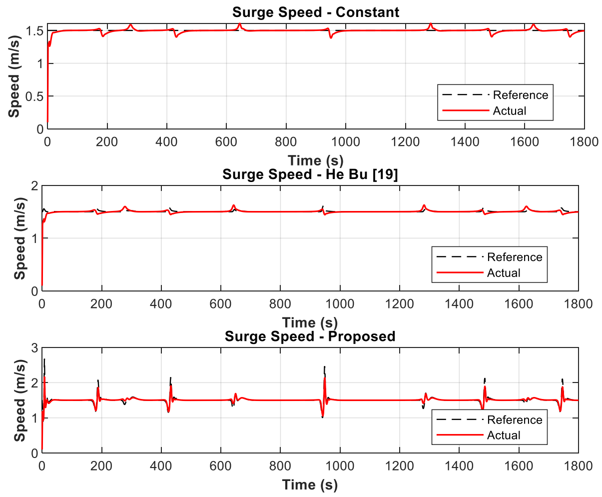

Fig. 5. Comparison of Surge speed on Curved Path Trajectory

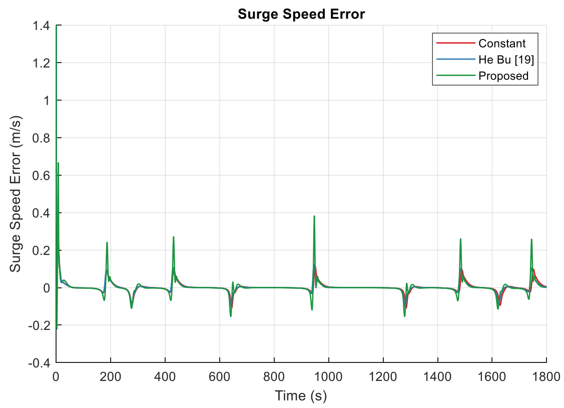

Fig. 6. Surge Speed Error Plot of Curved Path Trajectory

TABLE V. SURGE SPEED ERROR NUMERIC VALUE

Method	RMSE (m/s)	MAE (m/s)	STD (m/s)	MAX (m/s)
Constant	0.0356	0.0135	0.0354	0.1156
He Bu [19]	0.0357	0.0131	0.0355	0.1232
Proposed	0.0493	0.0169	0.0492	0.3823

Fig. 7 shows the comparison between the heading angle reference and the actual heading angle, as determined by ALOS, across various calculations of surge speed reference. The heading angle reference values correspond to the outputs of the ISS-ALOS block, as shown in Fig. 2. Heading angle error, illustrated in Fig. 8, is derived from comparing between the heading angle reference and the actual heading angle. The application of ISS-ALOS is typically seen as yielding reduced heading angle errors during turns relative to alternative computation methods, as evidenced between 160-180 s, 280-300 s, and 1250-1300 s. Table VI presents the RMSE, MAE, standard deviation, and maximum value of heading angle errors. The maximum value of heading angle error is determined analogous to the computation of the maximum surge speed Error.

TABLE VI. HEADING ANGLE ERROR NUMERIC VALUE

Method	RMSE (rad)	MAE (rad)	STD (rad)	MAX (rad)
Constant	0.0839	0.0260	0.0839	0.3528
He Bu [19]	0.0847	0.0262	0.0847	0.3556
Proposed	0.0808	0.0241	0.0808	0.3675

B. Square Path Trajectory

The square path in this test consists of waypoints linked by a linear trajectory. The waypoints are (0,0), (0,250), (250,250), (250,0), and (0,0). As demonstrated in (14), where (x_k, y_k) is the last waypoint passed and (x_{k+1}, y_{k+1}) is the waypoint being headed, the straight line linking the waypoints can be written as an equation of $x(\theta)$ and $y(\theta)$.

$$x(\theta) = x_k + (x_{k+1} - x_k)\theta \\ y(\theta) = y_k + (y_{k+1} - y_k)\theta \tag{14}$$

The ISS-ALOS parameters utilized in the square path test are presented in Table VII, whereas the He Bu [19] parameters are the same as those presented in displayed in Table III. The trajectory outcomes for each surge speed reference calculation on the square path are illustrated in Fig. 9. The utilization of ISS-ALOS effectively directs the USV to navigate through all waypoints, despite the trajectory consisting of sharp turns. Additionally, by using ISS-ALOS, the USV may avoid drifting too far from the path when making sharp turns because the XTE sharply increase, causing the speed to decrease. Fig. 10 presents further details, including the XTE plot for each distinct computation of the surge speed reference. Table VIII presents the RMSE, MAE, standard deviation, and maximum value of XTE on square path test.

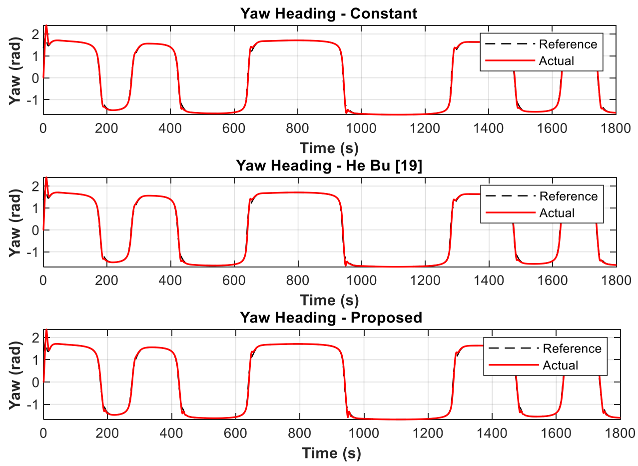

Fig. 7. Comparison of Heading Angle on Curved Path Trajectory

In certain segments, particularly when the XTE increases quickly, it is evident that ISS-ALOS can yield a lower peak value than the alternatives, succeeded by the constant surge speed reference and ultimately the equation given by He Bu [19]. This occurs because if the XTE increases rapidly, the surge speed reference must be decreased to prevent a significant rise in XTE. However, in the equation formulated by He Bu [19], an increase in XTE results in an elevation of surge speed reference, causing the USV to accelerate away from the trajectory when it should be decelerating.

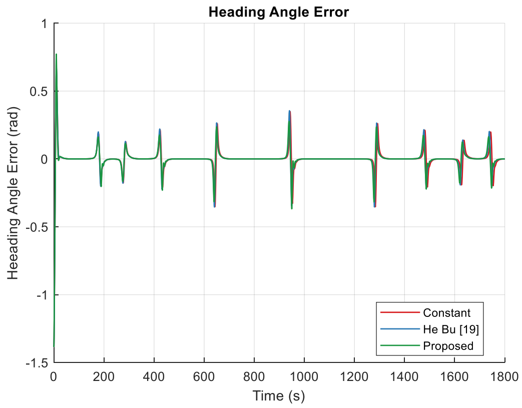

Fig. 8. Heading Angle Error Plot of Curved Path Trajectory

Fig. 11 illustrates the comparison between the surge speed reference and the actual surge speed. The surge speed reference in this figure corresponds to the output of the ISS-ALOS block, as shown in Fig. 2. ISS-ALOS provides higher surge speed reference compared to other methods, particularly when the USV approaches the path. But when the USV moves away, there is a reduction in velocity. The surge speed error can be computed by comparing the reference and surge speed with the actual surge speed. The corresponding plot is presented in Fig. 12, while the values for RMSE, MAE, standard deviation, and maximum value are detailed in Table IX. The maximum error speed is determined from the data recorded between 50 s and the end of the time. The higher surge speed error in ISS-ALOS result from its dynamic reference, which PID controller struggles to track. This is an intentional trade-off to prioritize minimizing XTE.

Fig. 13 displays a comparison between the heading angle reference and the actual heading angle determined using ALOS with various computations for the surge speed reference. The reference heading angles in this figure are produced by the ISS-ALOS block, as shown in Fig. 2. The comparison yields the heading error, illustrated in Fig. 14, with the RMSE, MAE, standard deviation, and maximum value presented in Table X. The determination of the peak heading angle error mirrors that of the maximum surge speed error. The higher heading error is caused by sudden changes in heading reference and reduced surge speed, which weaken yaw force and reduce the controller's responsiveness.

TABLE VII. ISS-ALOS SURGE SPEED REFERENCE PARAMETER

Parameter	Value
u_{min}	0.75
Δ_u	1.5
k_1	4
k_2	0.01
k_3	0.25
k_4	0.15

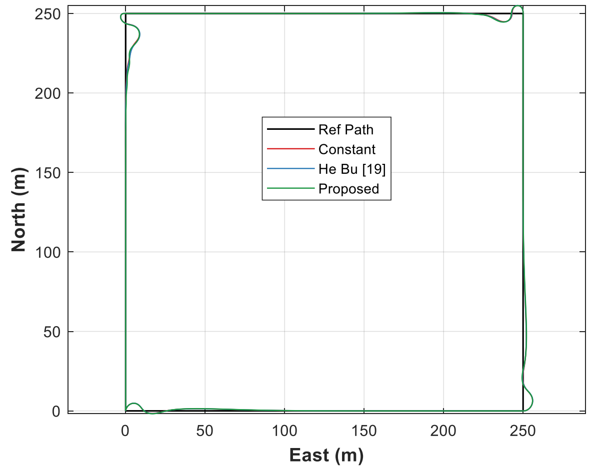

Fig. 9. Square Path Trajectory Result

TABLE VIII. XTE NUMERIC VALUE

Method	RMSE (m)	MAE (m)	STD (m)	MAX (m)
Constant	1.473	0.619	1.472	8.739
He Bu [19]	1.486	0.627	1.485	8.919
Proposed	1.443	0.627	1.442	8.651

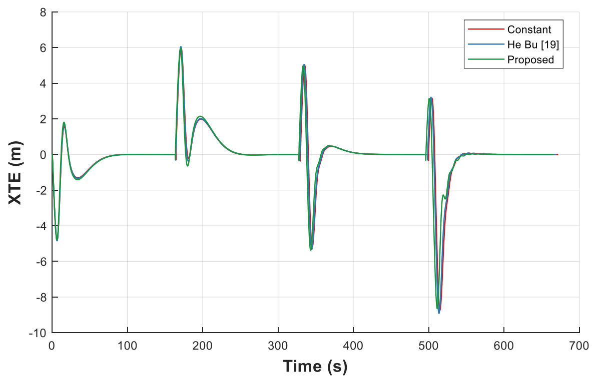

Fig. 10. XTE Plot of Square Path Trajectory

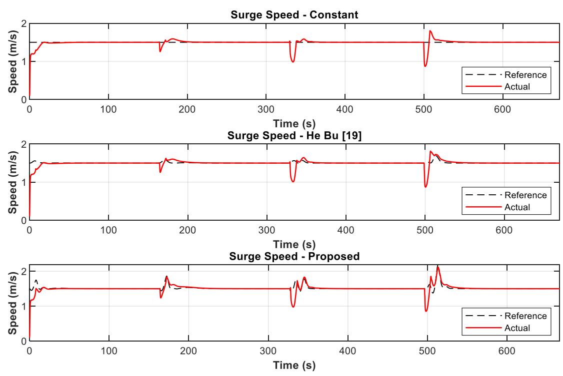

Fig. 11. Comparison of Surge speed on Square Path Trajectory

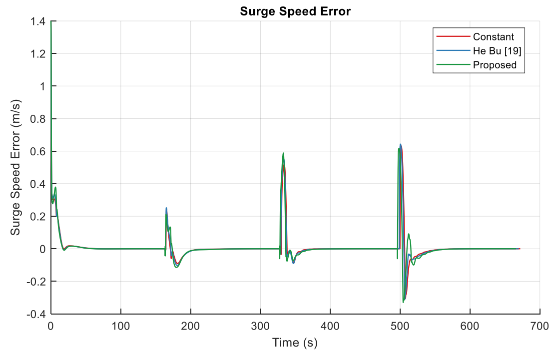

Fig. 12. Surge Speed Error Plot of Square Path Trajectory

TABLE IX. SURGE SPEED ERROR NUMERIC VALUE

Method	RMSE (m/s)	MAE (m/s)	STD (m/s)	MAX (m/s)
Constant	0.0865	0.0239	0.0860	0.6319
He Bu [19]	0.0896	0.0254	0.0891	0.6433
Proposed	0.0922	0.0275	0.0917	0.6159

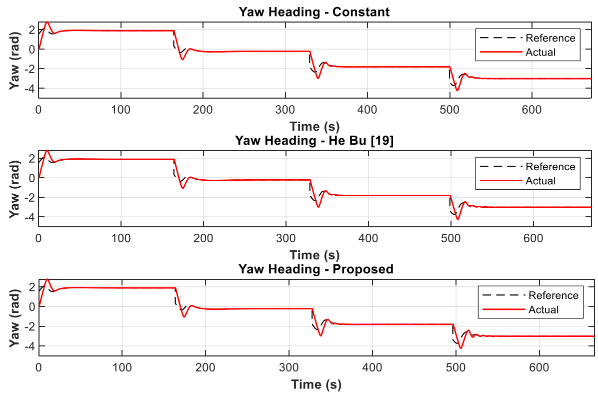

Fig. 13. Comparison of Heading Angle on Square Path Trajectory

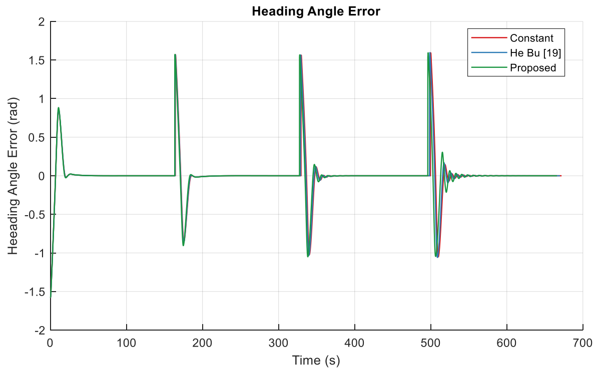

Fig. 14. Heading Angle Error plot of Square Path Trajectory

TABLE X. HEADING ANGLE ERROR NUMERIC VALUE

Method	RMSE (rad)	MAE (rad)	STD (rad)	MAX (rad)
Constant	0.2611	0.0767	0.2611	1.5928
He Bu [19]	0.2631	0.0778	0.2631	1.5968
Proposed	0.2641	0.7970	0.2642	1.5944

V. CONCLUSION

This study formulates the ISS-ALOS for path following. The computation of the surge speed reference depends on the path's curvature, XTE, and the rate of change of XTE. As the trajectory's curvature becomes more sharp, the velocity must be reduced. When the USV is distanced from the path, it must be accelerated to return to the path; conversely, if the USV is deviating from the path, its speed must be reduced. It is evident from the simulation results that using ISS-ALOS can guide the USV to follow the specified path and can prevent the XTE from being excessively large, particularly when the path bends sharply. Compared to existing methods, the proposed approach enhances path following performance by taking into account not only the path curvature but also the USV's motion tendency, whether it is moving toward or away from the path.

Future work includes adjusting heading control based on reference speed, such as speed-dependent lookahead, and exploring advanced controllers like MPC to enhance low-speed performance.

REFERENCES

[1] S. Wang, M. Sun, Y. Xu, J. Liu, and C. Sun, "Predictor-Based Fixed-Time LOS Path Following Control of Underactuated USV With Unknown Disturbances," *IEEE Transactions on Intelligent Vehicles*, vol. 8, no. 3, pp. 2088–2096, Mar. 2023, doi: 10.1109/TIV.2023.3245612.

[2] L. Martinović, Ž. Zečević, M. Bibuli, M. Caccia, and Đ. Nađ, "Adaptive Observer-Based Line-of-Sight Guidance Law for Path Following of Underactuated Unmanned Surface Vehicle With Sideslip Compensation," *IEEE Access*, vol. 12, pp. 144992–145002, 2024, doi: 10.1109/ACCESS.2024.3471790.

[3] E. Borhaug, A. Pavlov, and K. Y. Pettersen, "Integral LOS control for path following of underactuated marine surface vessels in the presence of constant ocean currents," in *2008 47th IEEE Conference on Decision and Control*, 2008, pp. 4984–4991. doi: 10.1109/CDC.2008.4739352.

[4] T. I. Fossen, K. Y. Pettersen, and R. Galeazzi, "Line-of-Sight Path Following for Dubins Paths With Adaptive Sideslip Compensation of Drift Forces," *IEEE Transactions on Control Systems Technology*, vol. 23, no. 2, pp. 820–827, Mar. 2015, doi: 10.1109/TCST.2014.2338354.

[5] T. I. Fossen, "An Adaptive Line-of-Sight (ALOS) Guidance Law for Path Following of Aircraft and Marine Craft," *IEEE Transactions on Control Systems Technology*, vol. 31, no. 6, pp. 2887–2894, Nov. 2023, doi: 10.1109/TCST.2023.3259819.

[6] L. Liu, D. Wang, and Z. Peng, "ESO-Based Line-of-Sight Guidance Law for Path Following of Underactuated Marine Surface Vehicles With Exact Sideslip Compensation," *IEEE Journal of Oceanic Engineering*, vol. 42, no. 2, pp. 477–487, Apr. 2017, doi: 10.1109/JOE.2016.2569218.

[7] Y. Su, L. Wan, D. Zhang, and F. Huang, "An improved adaptive integral line-of-sight guidance law for unmanned surface vehicles with uncertainties," *Applied Ocean Research*, vol. 108, p. 102488, Mar. 2021, doi: 10.1016/j.apor.2020.102488.

[8] S. Wu, H. Ye, W. Liu, X. Yang, Z. Liu, and H. Zhang, "An Improved ELOS Guidance Law for Path Following of Underactuated Unmanned Surface Vehicles," *Sensors*, vol. 24, no. 16, p. 5384, Aug. 2024, doi: 10.3390/s24165384.

[9] L. Ašanin, L. Martinović, Ž. Zečević, M. Bibuli, R. Ferretti, and M. Caccia, "Improved LOS Guidance Law for Path Following of Underactuated USV with Sideslip Compensation," in *2023 27th International Conference on Information Technology (IT)*, IEEE, Feb. 2023, pp. 1–4. doi: 10.1109/IT57431.2023.10078645.

[10] A. M. Lekkas and T. I. Fossen, "A Time-Varying Lookahead Distance Guidance Law for Path Following," *IFAC Proceedings Volumes*, vol. 45, no. 27, pp. 398–403, 2012, doi: 10.3182/20120919-3-IT-2046.00068.

[11] D. Mu, G. Wang, and Y. Fan, "A Time-Varying Lookahead Distance of ILOS Path Following for Unmanned Surface Vehicle," *Journal of Electrical Engineering & Technology*, vol. 15, no. 5, pp. 2267–2278, Sep. 2020, doi: 10.1007/s42835-020-00443-4.

[12] L. Wan, Y. Su, H. Zhang, B. Shi, and M. S. AbouOmar, "An improved integral light-of-sight guidance law for path following of unmanned surface vehicles," *Ocean Engineering*, vol. 205, p. 107302, Jun. 2020, doi: 10.1016/j.oceaneng.2020.107302.

[13] M. Li, C. Guo, and H. Yu, "Extended state observer-based integral line-of-sight guidance law for path following of underactuated unmanned surface vehicles with uncertainties and ocean currents," *Int J Adv Robot Syst*, vol. 18, no. 3, May 2021, doi: 10.1177/17298814211011035.

[14] Y. Li *et al.*, "Path-Following Control Based on ALOS Guidance Law for USV," *Electronics (Basel)*, vol. 14, no. 4, p. 749, Feb. 2025, doi: 10.3390/electronics14040749.

[15] X. Qu, X. Liang, Y. Hou, Y. Li, and R. Zhang, "Path-following control of unmanned surface vehicles with unknown dynamics and unmeasured velocities," *J Mar Sci Technol*, vol. 26, no. 2, pp. 395–407, Jun. 2021, doi: 10.1007/s00773-020-00744-3.

[16] Y. Shi, Y. Fan, D. Mu, and Y. Zhao, "Path Following Control of Unmanned Surface Vessel Based on Fixed Time Control Strategy," in *2023 42nd Chinese Control Conference (CCC)*, IEEE, Jul. 2023, pp. 2946–2951. doi: 10.23919/CCC58697.2023.10239772.

[17] Y. Yu, C. Guo, and T. Li, "Finite-Time LOS Path Following of Unmanned Surface Vessels With Time-Varying Sideslip Angles and Input Saturation," *IEEE/ASME Transactions on Mechatronics*, vol. 27, no. 1, pp. 463–474, Feb. 2022, doi: 10.1109/TMECH.2021.3066211.

[18] L. Li, Z. Pei, J. Jin, and Y. Dai, "Control of Unmanned Surface Vehicle Along the Desired Trajectory Using Improved Line of Sight and Estimated Sideslip Angle," *Polish Maritime Research*, vol. 28, no. 2, pp. 18–26, Jun. 2021, doi: 10.2478/pomr-2021-0017.

[19] H. Bu, Y. Fan, W. Sun, Y. Shi, and Z. Li, "Fixed-time path following control of unmanned surface vehicles subject to external disturbance and actuator saturation," in *2024 43rd Chinese Control Conference (CCC)*, IEEE, Jul. 2024, pp. 3060–3066. doi: 10.23919/CCC63176.2024.10661411.

[20] T. I. Fossen, *Handbook of Marine Craft Hydrodynamics and Motion Control*, Second. Trondheim, Norway: John Wiley & Sons Ltd, 2021.